

Sequestration of Methylene Blue and Lead Ions by MWCNT Modified with Polyconducting Polymers

A.A. Attia^{1*}, M.A. Shouman¹, S.M. Sayyah², N.A. Fathy¹,
A.B. Khaliel², K.M. Abas¹

¹National Research Center, Laboratory of Surface Chemistry and Catalysis, 33 El-Bohouth St., Dokki, Giza, Egypt, P.O.12622, ²Polymer Research Laboratory, Chemistry Department, Faculty of Science, Beni-Suef University, Egypt.

TAKING into consideration the perspective of green chemistry, an attempt was made to investigate regenerative material for carbon nanotubes (CNTs) with high productivity. The special properties of CNTs, such as easy functionalization ability, high surface area, and unique thermal, mechanical, and electrical properties, make them an appealing component for composite materials, which resulted in the attraction of great interest on CNT-based composites. This research work focuses mainly on multiwall carbon nanotubes (MWCNTs) synthesized from camphor over iron nitrate catalyst supported on alumina by wet impregnation method. The formation of MWCNTs and incorporation of poly conducting polymers (o- and m-Toluidine) on the surface of MWCNTs was confirmed by high resolution transmission electron microscope (HRTEM), X-ray diffraction (XRD), Fourier transform infrared (FTIR), Ultraviolet visible spectroscopy (UV-Vis), low temperature nitrogen adsorption and Thermo-Gravimetric analysis (TGA). The performance evaluation of as-synthesized MWCNTs showed maximum adsorption towards methylene blue (MB) dye while the nanocomposites samples revealed maximum adsorption for the Pb(II) ions. MWCNTs and their nanocomposites pose a great potential as a promising material for application in adsorption from aqueous solution.

Keywords: MWCNT, Conducting polymers, Nanocomposite, adsorption, Dye, Heavy metal.

The human impact on the environment and the increase in the fossil resources price, in addition to its ever-aggravation impact on global warming have been an area of immense interest over the past decades. This led to extensive research to produce new environmental friendly materials [1]. The discovery of CNT has led to an outburst research in nanoscience and nanotechnology. Applications of CNT in various domains of technology including drugs, electronic nanodevices[2], fillers [3] and various applications in biomedicine [4], fuel cells, and semiconductor devices[5] have also been described. The properties of CNTs depend not only on the arrangement of their graphitic rings and the diameter of their helical structure, but also on the starting precursor too[6]. For different sorts

*Corresponding author: E-mail address: amina_abdelmeguid@yahoo.com

DOI: 10.21608/ejchem.2017.564.1003

© 2017 The National Information & Documentation Center (NIDOC)

of deposition procedures, graphite target and petroleum products are in practice, used as precursors for synthesizing CNTs [7]. As indicated by the role of green chemistry, the food supply of any industrial procedure must be renewable, instead of exhausting a natural asset. In addition, the process must be modeled to achieve maximum consolidation of the constituent atoms (feed stock) into the final product. Subsequently, there has been a growth in exploring new natural renewable precursors with low cost for CNTs synthesis to achieve high efficiency. Camphor ($C_{10}H_{16}O$) is an attractive new material that readily ignites and burns without producing any residues. It consists of both sp^2 and sp^3 carbons while graphite contains sp^2 carbon only. Also, the presence of oxygen rich in camphor structure helps in oxidizing the amorphous carbon in situ. This gives camphor an advantage for CNTs – based preparation [8].

Catalyst has a great influence on CNTs integration and is the dominant factor that controls the structure of CNTs.

Metals such as Fe, Co, and Ni have stronger adherence with the growing CNTs than other transition metals. Thus, they are capable in forming CNTs with low diameter. The textural properties and the surface morphology of the substrate material highly affects the quality and the yield of the obtained CNTs. Alumina materials are accounted to be a superior catalyst support as result of the strong metal-support interaction. This permits high metal scattering with high density of catalytic sites [9]. Such interaction keeps metal species from accumulation and forming undesirable vast bunches that prompt graphite particles or defective MWCNTs [10].

Owing to the weak dissipation and insolubility of CNTs in common solvents and matrices, these features have restricted their application. The modification of CNTs by polymers is a significant method used to increase the dispersion of nanotubes. Conducting polymers has received special new possibilities for fabricating devices such as batteries, electrochromic displays and sensors [11]. One of the conducting polymers such as o- and m – toluidine has gained interest by researchers due to their good process ability, environmental stability and reversible control of conductivity both by charge–transfer doping and protonation [12,13]. The utilization of conducting polymers with CNTs to form nanocomposites creates materials with extraordinary properties [14]. Recently some investigators direct their research toward the application of MWCNTs/ conducting polymer nanocomposites for water remediation and the removal of heavy metal ions from aqueous solutions [15,16].

This objective of this study gives prior concern on the synthesis of MWCNT/ Fe catalyst supported on alumina using renewable natural camphor via chemical vapor deposition (CVD). The obtained MWCNTs incorporated by in situ oxidative chemical polymerization of two monomers [2-methylaniline (o-Toluidine) and 3-methylaniline (m-Toluidine)] using ammonium peroxydisulphate as an oxidant in

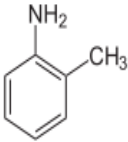
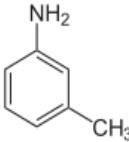
the presence of HCl as a dopant. The potential for MWCNTs and nanocomposites were estimated towards the removal of lead (II) ion and methylene blue dye from aqueous solutions. Adsorption capacity was measured via batch model. The data obtained were simulated by Langmuir and Freundlich isotherm models.

Materials and Methods

Materials

All chemicals were of analytical grade and purchased from Merck and Fluka. Camphor (C₁₀H₁₆O) was locally collected. Conducting polymers (o- and m-Toluidine) were distilled under vacuum at 180°C. The metal stock solution of Pb(II) (100 mg/L) was prepared by dissolving its nitrate salt in deionized water. The solution was further diluted to the required concentrations for the sorption measurement at pH= 5.5. Methylene Blue (MB) dye stock solution was prepared by dissolving an accurately weighed dye in distilled water to give concentration 100mg/L. The initial concentrations of the dye solutions were performed by diluting the stock solution to concentrations varying from 20 to 100 mg/L. The physical properties of camphor and the two conducting polymers are given in Table 1.

TABLE 1. Physical properties of camphor and monomers.

Name	Camphor	o-Toluidine	m-Toluidine
Molecular structure			
IUPAC name	1,7,7-Trimethylbicyclo [2.2.1]heptan-2-one	2-methylaniline	3-methylaniline
Molecular formula	C ₁₀ H ₁₆ O	C ₇ H ₉ N	C ₇ H ₉ N
Molar mass	152.23 g.mol ⁻¹	107.17 g/mol	107.17 g/mol
Density	0.992 g .cm ⁻¹	1.00 g/cm ³	0.98 g/cm ³
Melting point	175°C (374°F ; 448°K)	-14.41 deg C(6°F;258.6 °K)	-31.3 deg C(-23 °F ;241.7°K)

Physico – chemical characterization

The measurement of Pb(II) concentration was analyzed by using an atomic absorption spectrophotometer supplied by Perkin Elmer, Model AAnalyst 200. The crystalline structure was determined using X – ray diffraction spectroscopy (XRD Rigaker 1710) employing CuK α radiation from 10° <2 θ <90° with a scanning speed of 2° min⁻¹. In addition, the surface functional groups were identified using Infra – red analysis spectrophotometer (FTIR – 6100, Jasco) by

KBr pellet method. The spectra were recorded from 4000 to 400 cm^{-1} . The thermal profile was detected in a N_2 atmosphere using TG and DTG curves (Perkin Elmer 7HT). To study the surface textures, the morphology was detected by using Scanning electron microscopy analysis (Model JEM-2100). The specific surface area was measured using the BET method, which involves physisorption of gas multilayer on the particle surface (Quantachrome Autosorb NOVA-version 1.12). The ultraviolet visible (UV-Vis) spectra were recorded over a range 200 – 800 nm using UV – Vis 240C spectrophotometer.

Catalyst preparation

In this study, the catalyst was prepared using the wet impregnation method [17] with $\text{Fe}(\text{NO}_3)_2 \cdot 9\text{H}_2\text{O}$ to obtain a catalyst with 5 wt% supported on alumina. The solvent was then evaporated and the resultant cake heated to 100°C. The resulted catalyst was then calcined for 3hr at 700°C and 800°C.

Synthesis of MWCNTs

The experimental set up is based on a horizontal electronic furnace used to cover the stainless steel tube during MWCNTs fabrication. Camphor as a precursor was introduced to the inlet of the stainless steel tube fitted by the first furnace to release the vaporized MWCNTs. The reaction temperature was increased to 250°C and maintained at this temperature for 30 min to ensure that the precursor was completely pyrolyzed. The chemical vapor deposition (CVD) experiments commenced when the deposition temperature of the second furnace reached the optimum temperature (850°C) where the catalyst acts as the substrate. The exhaust nitrogen gas in the stainless steel tube induced the movement of the amorphous vaporized carbon by means of a mass flow controller, thereby allowing MWCNTs on the surface of the proposed substrate [18]. The as-synthesized MWCNTs were purified with 5M HNO_3 and HCl. The reaction flask was equipped with a reflux condenser on a magnetic stirrer at 100°C for 4hr. The mixture was then cooled to the room temperature, filtered, washed with deionized water and dried in an air oven over night at 100°C. The yield of MWCNTs for the catalyst prepared at 700°C was greater than that calcined at 800°C, thus all experiments were conducted using the conditions for greater yield.

Synthesis of MWCNTs/Nanocomposite

Nanocomposite samples were synthesized using in situ oxidative chemical polymerization on the MWCNTs. The polymerization of both monomers (o-Toluidine and m-Toluidine) was carried out in distilled water using HCl as a dopant and $(\text{NH}_4)_2\text{S}_2\text{O}_8$ as an oxidant. The purified MWCNTs (500 mg) was placed into round-bottom flask with 10 ml deionized water and sonicated for 1 hr to form uniform suspension. Ammonium persulphate [$(\text{NH}_4)_2\text{S}_2\text{O}_8$, 0.6 M, 6.85 gm] was dissolved in 15 ml distilled water and then dropped onto the purified MWCNTs solution with continuous stirring for 15 min. o-Toluidine monomer (0.2M, 1.1 ml) was then mixed with HCl (0.25M, 1.1 ml). This solution was added drop wise onto the mixture under ultrasonic water bath and vigorous

stirring at room temperature for 1 hr. The synthesized MWCNTs/conducting polymer (o- toluidine) was filtered and rinsed several times with deionized water. The nanocomposite powder was dried overnight in an air oven at 60°C. The same procedure was repeated for (m-toluidine) monomer using (NH₄)₂S₂O₈ (4.56 gm, 0.4M), m-toluidine (0.55 ml, 0.1 M) and HCl (0.44 ml, 0.1 M).

Batch experiments

Batch adsorption experiments were performed using 10 mg of MWCNTs and nanocomposite samples were added to 10 ml of varying concentration (20 – 100 mg/L) including Pb(II) ions (pH 5.5) and methylene Blue dye (MB). The resultant mixture was shaken for 24 hr. The amount of Pb(II) and MB (mg/g) adsorbed per unit mass of the adsorbent (mg/g) at equilibrium is obtained by equation 1:

$$q_e = V (C_i - C_e) / m \quad (1)$$

where C_i is the initial concentration of Pb(II) and MB in solution (mg/L), while C_e is the concentration of Pb(II) and MB in solution at equilibrium, q_e is the amount of solute adsorbed per unit weight of adsorbent (mg/g), m is the mass of the adsorbent (mg) and V is the volume of the Pb(II) and (MB) solution (mL).

Results and Discussion

X-Ray diffraction

X-ray diffraction is conducted to determine the phase and phase purity for the investigated samples. Figure 1.(a) displays the XRD pattern of the catalysts under investigation. Three characteristic peaks centered around 2θ (14.9°, 28° and 48.7°) were perfectly indexed for pure boehmite (JCPDS card 01-083-2384). The presence of alumina was confirmed by the presence of the boehmite phase present [19]. On the other hand, the X-ray diffraction peaks centered at 2θ (32°, 38° and 42°) were ascribed to the diffraction pattern of ferric oxide (hematite, JCPDS card 33-0664). Figure 1. (b) ascribed the XRD pattern of the synthesized MWCNTs, which showed two major peaks at 2θ (26° and 44°). These peaks correspond to the graphite, which is attributed to the graphitic structure of MWCNTs [20]. Figure 1. (c, d, e and f) shows the XRD patterns of the conducting polymers and their nanocomposites, respectively. These peaks reveal low crystallinity with a characteristic peak observed at 2θ (25°). This result was ascribed to the benzenoid and quinoid structures in aniline rings of Emeraldine salt of the polymer producing large amorphous regions. The slight movement in the top positions of this peak at the nanocomposites may be attributed to charge transfer interaction between conducting polymers and MWCNTs producing varieties in chain designs [21].

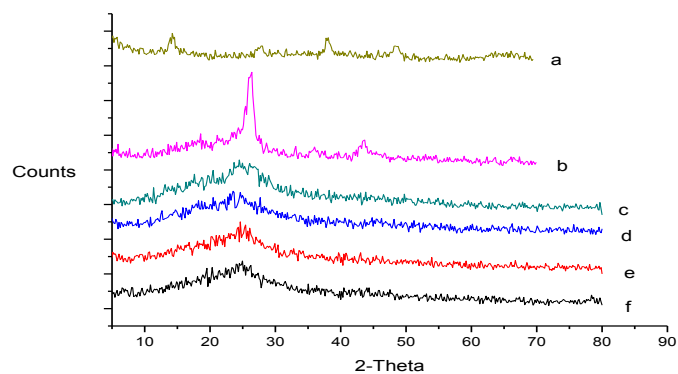


Fig. 1. XRD diffraction of a) catalyst, b) MWCNTs, c) o - Toluidine, d) m - Toluidine, e) MWCNTs/nanocomposite (o-Toluidine), f) MWCNTs/ nanocomposite (m - Toluidine).

FTIR analysis

The FTIR – spectrum for the synthesized MWCNTs (Fig. 2a) showed a broad peak at about 3446 cm^{-1} which could be assigned to the O-H stretching from carboxyl groups ($\text{O}=\text{C}-\text{OH}$, $\text{O}=\text{C}$ or $\text{C}-\text{OH}$), while the peak at $2921\text{--}2856\text{ cm}^{-1}$ can be correlated to the O-H stretching from strongly hydrogen bonded $-\text{COOH}$ [22]. The peaks at 1624 cm^{-1} are relative to the characteristic $\text{C}=\text{C}$ stretching. This finding confirms the hexagonal structure of the MWCNTs [23]. The spectrum of both conducting polymers showed common characteristics stretching vibration peaks at 1571 cm^{-1} ($\text{C}=\text{C}$ quinoid rings), 1479 cm^{-1} ($\text{C}=\text{C}$ benzenoid rings), 1260 cm^{-1} ($\text{C}-\text{N}$) and 1038 cm^{-1} ($\text{C}-\text{H}$) in Fig. 2.(b, c).

Figure 2. (d, e) represent the nanocomposite samples. The peaks of both polymers chains were shifted to longer wavelengths. This implies that there is an interaction between quinoid rings and MWCNTs [24]. The FTIR-spectrum of all the investigated samples is summarized in Table 2.

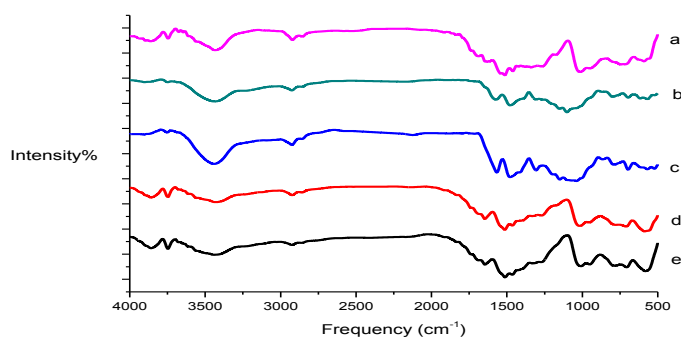


Fig. 2. FTIR spectra of; a) MWCNTs, b) o-Toluidine, c) m-Toluidine, d) MWCNTs/ nanocomposite (m-Toluidine), e) MWCNTs/ nanocomposite (o- Toluidine).

TABLE 2 . FTIR absorption bands of the prepared samples.

Frequency (Cm ⁻¹)					Assignments
MWCNT-Fe/Al/700	MWCNT/oTol	o - Tol	MWCNT/m - Tol	m - Tol	
-----	558.291 ^w 586.254 ^w	568.998 ^b 617.109 ^b	582.397 ^b	522.615 ^m 567.934 ^b 607.467 ^w	Bending deformation of N-H group attached to benzene ring
-----	710.64 ^b 779.101 ^{sh} 954.591 ^b 1018.23 ^b	617.109 ^b 696.17 ^b 756.923 ^{sh} 797.421 ^b 868.774 ^b 1038.48 ^{sh} 1102.125 ^s	From: 706.783 ^b To: 1008.59 ^b	From: 696.177 ^s To: 1149.37 ^m	Out of plane C-H deformation of 1,2,4-tri substitution in o-Tol and 1,3,4-trisubstitution in m-Tol
950.734 ^b 1015.34 ^b	954.531 ^b 1018.23 ^b	-----	951.698 ^m 1008.59 ^b	-----	O-H bending in MWCNTs
1175.41 ^m	1200 ^{sh}	-----	1200 ^{vssh}	-----	Prove that the band observed at about 1700 cm ⁻¹ is due to carboxylic group
1267.97 ^b	1270.86 ^b	1206.26 ^{sh} 1261.22 ^b 1306.54 ^b	1272.79 ^w	1307.5 ^s	C-O stretching for MWCNTs and symmetric stretching vibration for C-O or C-N for polymer
1459.85 ^s	1464.67 ^m	-----	1464.67 ^s	-----	C-H stretching
1514.81 ^s 1541.81 ^m	1514.81 ^s	-----	1512.88 ^s	-----	C=O carbonyl group'MWCNTs'
1685.48 ^b	1685.48 ^{sh}	-----	1688.37 ^{sh}	-----	Can be attributed to ester group or carboxylic group
1642.09 ^m	1644.98 ^m	1479.13 ^b 1571.7 ^b	1644.98 ^s	1479.13 ^b 1566.88 ^s	Due to C=C in MWCNTs and stretching vibration of C=C in benzene ring or C=N in quinoid unite for polymer

1685.48 ^b 1833.97 ^b	1685.48 ^{sh} 1832.04 ^w	-----	1688.37 ^{sh} To: 1832.04 ^w	-----	Due to C=O
2856.06 ^m 2921.63 ^m	2857.99 ^b 2923.56 ^m	2857.99 ^b 2925.48 ^m	2859.92 ^b 2925.48 ^b	2858.95 ^b 2925.48 ^m	Due to C-H stretching of MWCNTs or N-H symmetric stretching vibration in polymer
-----	-----	3234.04 ^w	-----	3094.23 ^w	Stretching vibration of C-H aromatic for polymer structure
3434.6 ^b	3425.92 ^b	3440.39 ^{v.b}	3441.35 ^b	3441.35 ^{v.b}	Asymmetric stretching vibration of N-H in polymer and O-H stretching for MWCNTs
-----	3747.98 ^s	3749.9 ^m	3747.01 ^s	3752.8 ^b	Stretching vibration of O-H group in polymer

Thermo-gravimetric analysis

Thermo-gravimetric analysis was performed to characterize the thermal behavior of the investigated samples. All the samples revealed similar decomposition curves. Figure 3.(a) represents the TGA curve for the MWCNTs. The weight reduction was observed at temperature less than 100°C. However, the temperature between 150 - 400°C was consistent with the degradation of absorbed water and oxygen functional groups, respectively. The presence of -COOH groups on the walls of MWCNTs not only enhanced the dispersibility, but also could anchor the conducting polymers to the surface. Figure 3. (b,c) demonstrate the TGA curves for both conducting polymers. The gradual weight loss between 100 - 200°C was attributed to the deprotonation of the dopant HCl. The significant weight loss (~ 29%) between 400 - 600°C was assigned to the degradation and decomposition with different degree of polymerization [24]. For the nanocomposite samples (Fig. 3.d, e), the gradual decomposition below 200 was ascribed to the evaporation of adsorbent solvent in addition to the decomposition of oxygen groups on the MWCNTs. Moreover, the weight loss around 400 - 600°C, exhibited degradation and decomposition of the conducting polymers. Overall, these results indicate that the nanocomposite samples have higher thermal stability than the conducting polymer. This result confirmed the strong interactions between MWCNTs and polymers which impose a restriction on the decomposition of the -COOH groups remaining on the MWCNTs surface [25].

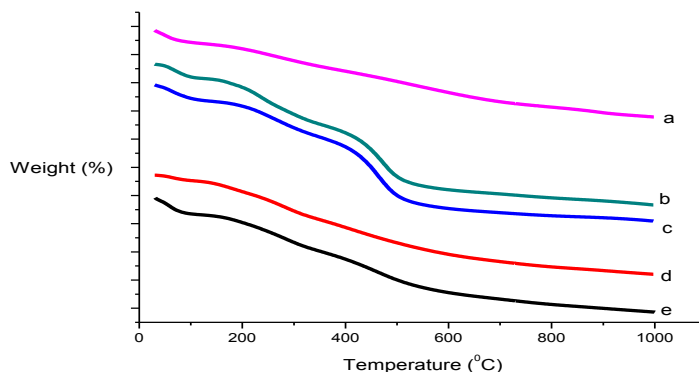


Fig. 3. TGA spectra of; a) MWCNTs, b) o - Toluidine, c) m - Toluidine, d) MWCNTs/ nanocomposite (o-Toluidine) e) MWCNTs/ nanocomposite (m - Toluidine).

Morphological analysis

Figure 4.(a) shows the SEM images of synthesized MWCNTs. As seen from the observed micrographs that the MWCNTs is grown of homogeneous and dense distribution of a web-like network with diverse orientations and some entanglements. However, more detailed morphology of the MWCNTs can be observed using the HRTEM images (Fig.4.b). It can be discerned from (Fig. 4 b) that the tubular structure of nanotubes was found with an average of outer diameter 116.2 nm and inner diameter of 32.7 nm. Additionally, there are some carbon spheres attached to the ends of some nanotubes which appear as dark dots inside the body of nanotubes and on its surface during the synthesis process [26].

The HRTEM micrographs of both polymers (Fig. 4. c, d) show non-uniform size of spherical shape and interconnected particles which are in a size range between 200-500 nm in diameter. Figure 4. (e, f) display a homogeneous coating of polymers onto the MWCNTs, proving that MWCNTs were well dispersed in the polymer matrix. A new interwoven fibrous structure of diameter range between 0.5 μm - 200 nm was exhibited for the nanocomposite, respectively.

BET surface area

The surface characteristics of all the investigated samples are summarized in Table 3. As revealed from this table that the surface area of MWCNTs decreases after being subjected to the conducting polymers from 207.2 to 203 and 126 m^2/g for MWCNTs and nanocomposites, respectively. This decrease accompanied with minute change in total pore volume and pore diameter. The incorporation of conducting polymers onto the MWCNTs reduced the specific surface area due to the occupation of the pores by the polymers. This leads to the blockage in the porous network and / or occupy the inner pores of the MWCNTs during the modification process [27].

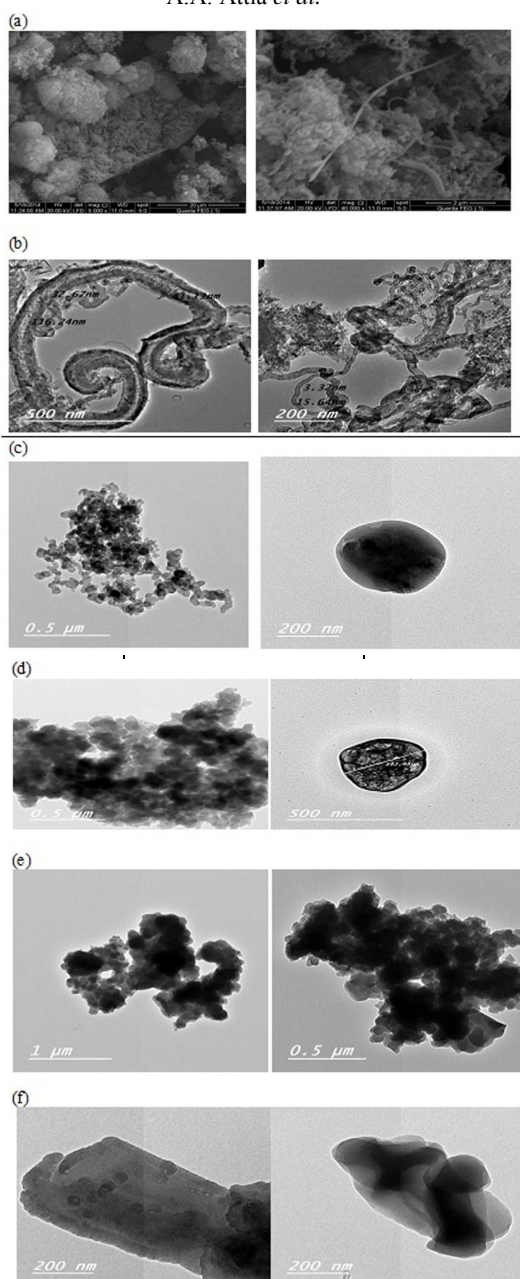


Fig.4. SEM of :a) MWCNTs and HRTEM of :b) MWCNTs, c) o- Toluidine, d) m - Toluidine, e) MWCNTs/ nanocomposite (o-Toluidine), f) MWCNTs/ nanocomposite (m-Toluidine).

TABLE 3 . Textural properties of the prepared samples.

Sample	MWCN Ts	o - Tol	MWCNTs/ nanocomposite (o - Tol)	m - Tol	MWCNTs/P- nanocomposite
Surface area (m ² /g)	207.2	64.1	203	84.2	126
Total pore volume (cm ³ /g)	0.11	0.05	0.10	0.04	0.09
Average pore diameter(Å)	20.3	14.1	17.3	18.7	20.2

UV-Vis absorption analysis

UV-Vis spectroscopy was utilized to understand the electronic states of both polymers and the nanocomposite samples. The standard oxidative polymerization for synthesis of both pure conducting polymers and their related nanocomposites were studied to explain the presence of dispersed MWCNTs into the medium of reaction could effect on the polymer chains oxidation ratio to the final products of synthesis. For this reason, it was studied the UV-Vis spectra to verify the amount of quinone-like structure per repeat unit [28].

Figure 5. (a, b) of both polymers showed two characteristic bands at 350nm and 600 nm. The first peak corresponds to π - π^* transition to the backbone of both polymer chain [29] indicating that the resulting that (o- and m-Toluidine) emeraldine salt was in the doped state. However, the peak at 600 nm may be due to the high conjugation of the aromatic polymeric chain. As MWCNTs were incorporated into both polymers in Fig. 5 (c, d) the characteristic peaks of both polymers were shifted to longer wave length at 620 nm indicating the interaction between quinoid rings and MWCNTs [30]. Also, the π - π^* transition of both polymers in the nanocomposites was also shifted to longer lengths at 380 nm.

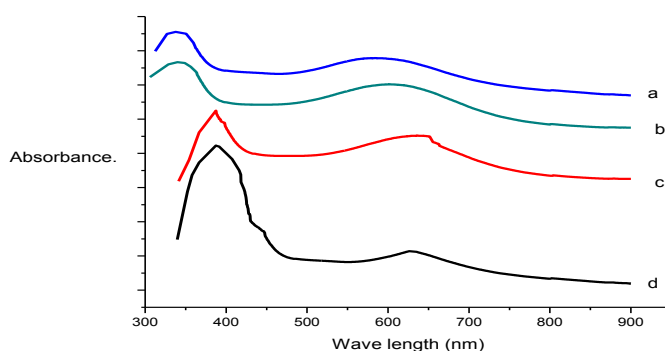


Fig. 5. UV-Vis spectra of; a) o - Toluidine, b) m- Toluidine, c) MWCNTs/nanocomposite (o - Toluidine) , d) MWCNTs/nanocomposite (m - Toluidine).

Adsorption isotherms

Adsorption isotherms were applied to receive information on the capacity of the adsorbent and also on the nature of the solid – surface interaction. Two isotherm models (Langmuir and Freundlich) were used to describe the experimental data. Langmuir isotherm [31] is described in equation 2 :

$$C_e/q_e = 1/K_L \cdot q_{\max} + C_e/q_{\max} \quad (2)$$

where C_e is the equilibrium concentration (mg/L) of (MB) dye and Pb(II), q_e is the uptake of (MB) dye and Pb(II) ions at equilibrium (mg/g), q_{\max} is the adsorption capacity of the tested nanomaterial samples (mg/g) and K_L is a Langmuir constant (L/mg) related to the free energy of adsorption.

The essential characteristics of the Langmuir isotherm can be described by a separation factor as shown in equation 3:

$$R_L = 1 / (1 + K_L \cdot C_0) \quad (3)$$

where R_L is the dimensionless equilibrium parameter and C_0 is the initial adsorbate concentration. Adsorption process was favorable based on the separation factor, when $(0 < R_L < 1)$ is favorable, $(R_L = 1)$ is linear, unfavorable when $(R_L > 1)$ or irreversible when $(R_L = 0)$.

Freundlich isotherm is an empirical model that considers heterogeneous adsorptive energies on the surface of adsorbent, and it can be described as equation 4 [32] :

$$q_e = K_F \cdot C_e^{1/n} \quad (4)$$

where K_F (mg/g) (L/mg)^{1/n} and n are the Freundlich constant, which indicate the capacity and power of adsorption, respectively.

The Langmuir and Freundlich parameters were calculated and collected in Tables 4, 5. It is clear from this Table and Fig.6 that MWCNTs have the highest adsorption capacity for MB dye. This trend is attributed to the fact that the surface of MWCNTs has substantial amounts of carbonyl groups that react with MB. Another reason may be due to the large specific surface area of MWCNTs that greatly affects on the adsorption ability or the voids present in the MWCNTs may also favor the adsorption of MB. However, the modification of synthesized MWCNTs tends to lower the surface area, this finding indicates that the nanocomposite samples can't be fully accessed by the dye molecule due to the pore blockage. This clearly effects on their adsorption behavior towards the MB dye [33]. On the contrary for Pb(II) adsorption system , the nanocomposite samples portrayed high adsorption capacity referring to Fig. 7. The optimum pH for adsorption of Pb(II) was carried out at pH=5.5. At this pH, the most possible mechanism postulated is the reaction between electron pair in nitrogen (amine

functional group) and the methyl group of both polymers with the metal ion which leads to the formation of metal complex. At this stage, the polymer is changed into an undoped form, then, the free amine or imine will be accessible to metal chelating. So, the adsorption of Pb(II) ions will be increased significantly [34,35].

According to the values of correlation coefficient (R^2) and the separation factor (R_L) for both systems, MB and Pb(II) ions (Table 4 & 5), the equilibrium data was fitted to the Langmuir model (Fig. 6,7). This indicates the homogeneous nature of the adsorption sites onto the tested samples. It is obviously shown from Tables 4, 5 that the position of methyl group present in both polymers (o- and p- toulidine) didn't greatly affect on the adsorption capacities of both nanocomposites toward the adsorption of MB and Pb(II) ions. Table 6 represents a comparison between our work and some recently reported researchers. From this table, the investigated samples of the present study exhibit good porosity characteristics and recommend the potential usage for waste water treatment.

TABLE 4. Langmuir and Freundlich parameters for MB adsorption system.

Adsorbent	Langmuir model				Freundlich model		
	K_L (L/gm)	q_0 (mg/g)	R^2	R_L (mg/L)	K_F (mg/g)	N	R^2
MWCNTs	0.2	125	0.99	0.05	22	2.2	0.92
o - Tol	0.02	19.6	0.98	0.4	5.5	0.9	0.91
MWCNTs/nano Composite (oTol)	0.06	40	0.99	0.14	5.2	2.3	0.90
m - Tol	0.007	40	0.99	0.6	1.8	1.4	0.93
MWCNTs/nano Composite (mTol)	0.012	47.6	0.98	0.42	1.2	1.2	0.91

TABLE 5. Langmuir and Freundlich parameters for Pb(II) adsorption system.

Adsorbent	Langmuir model				Freundlich model		
	K_L (L/gm)	q_0 (mg/g)	R^2	R_L (mg/L)	K_F (mg/g)	n	R^2
MWCNTs	0.11	83.3	0.99	0.08	11.6	2	0.91
o - Tol	0.07	66.7	0.98	0.12	6	1.7	0.95
MWCNTs/nano composite(oTol)	0.28	100	0.99	0.03	25.1	2.6	0.88
m - Tol	0.13	37	0.99	0.07	5.8	2.0	0.92
MWCNTs/ nano composite(mTol)	0.39	88.3	0.99	0.02	26	3.1	0.90

TABLE 6 . Comparison of the equilibrium adsorption capacity of various modified CNTs as adsorbents for MB dye and Pb(II) cation.

Adsorption of Methylene blue dye		
Adsorbent	q ₀ (mg/g)	References
Starch-MWCNT magnetic functionalization	93.7	[36]
MWCNT-Magnetic composite	11.86	[37]
MWCNT/Magnetic-modification	48.1	[38]
MWCNTs	125	This work
MWCNTs/P-oTolnanocomposite	40	This work
MWCNTs/P-mTolnanocomposite	47.61	This work
Adsorption of lead (II) cation		
Adsorbent	q ₀ (mg/g)	References
MWCNTs-TAA (TAA); Tris (2-aminoethyl) amine	71	[39]
Oxidized-MWCNT	27.8	[39]
MWCNTs-COOH	54.38	[40]
MWCNTs	83.33	This work
MWCNTs/P-oTolnanocomposite	100	This work
MWCNTs/P-mTolnanocomposite	83.33	This work

Conclusions

Multiwalled carbon nanotubes (MWCNTs) were successfully synthesized through chemical vapor deposition (CVD) of camphor, as an unconventional natural precursor using ferric nitrate supported on alumina as a catalyst. Nanocomposite samples were successfully prepared through in-situ oxidative chemical polymerization of (o- and m-Toluidine). These samples exhibited a good interaction between MWCNTs and both polymers based on the shift in the electronic transition described by UV-Vis and FTIR spectra inferred in quinoid rings. SEM revealed the incorporation of MWCNTs with both polymers. The MWCNTs displayed the highest adsorption capacity of MB dye. However, the nanocomposite samples had the highest adsorption capacity for the Pb²⁺ through chelating agent. The equilibrium data fitted well with the Langmuir model.

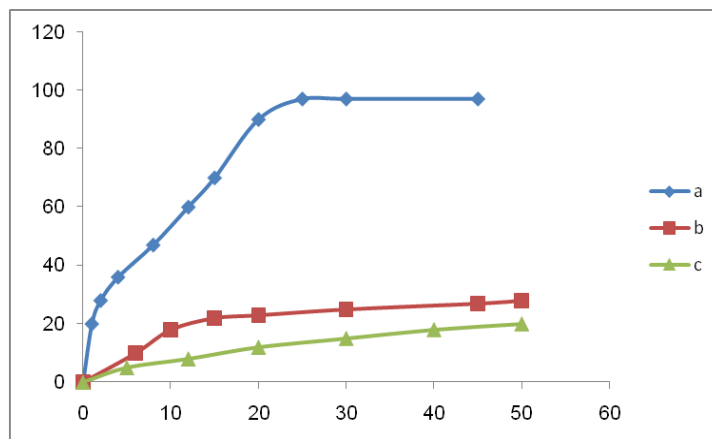


Fig.6. Adsorption isotherm for MB onto (a) MWCNTs (b) MWCNTs/nanocomposite (o-Toluidine) and (c) MWCNTs/nanocomposite (m-Toluidine).

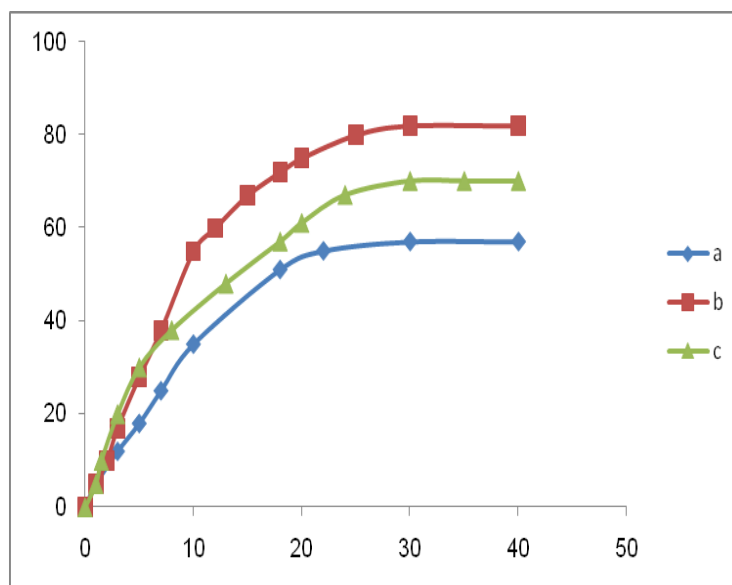


Fig. 7. Adsorption isotherm for Pb²⁺ onto (a) MWCNTs (b) MWCNTs/nanocomposite (o-Toluidine) and (c) MWCNTs/nanocomposite (m-Toluidine).

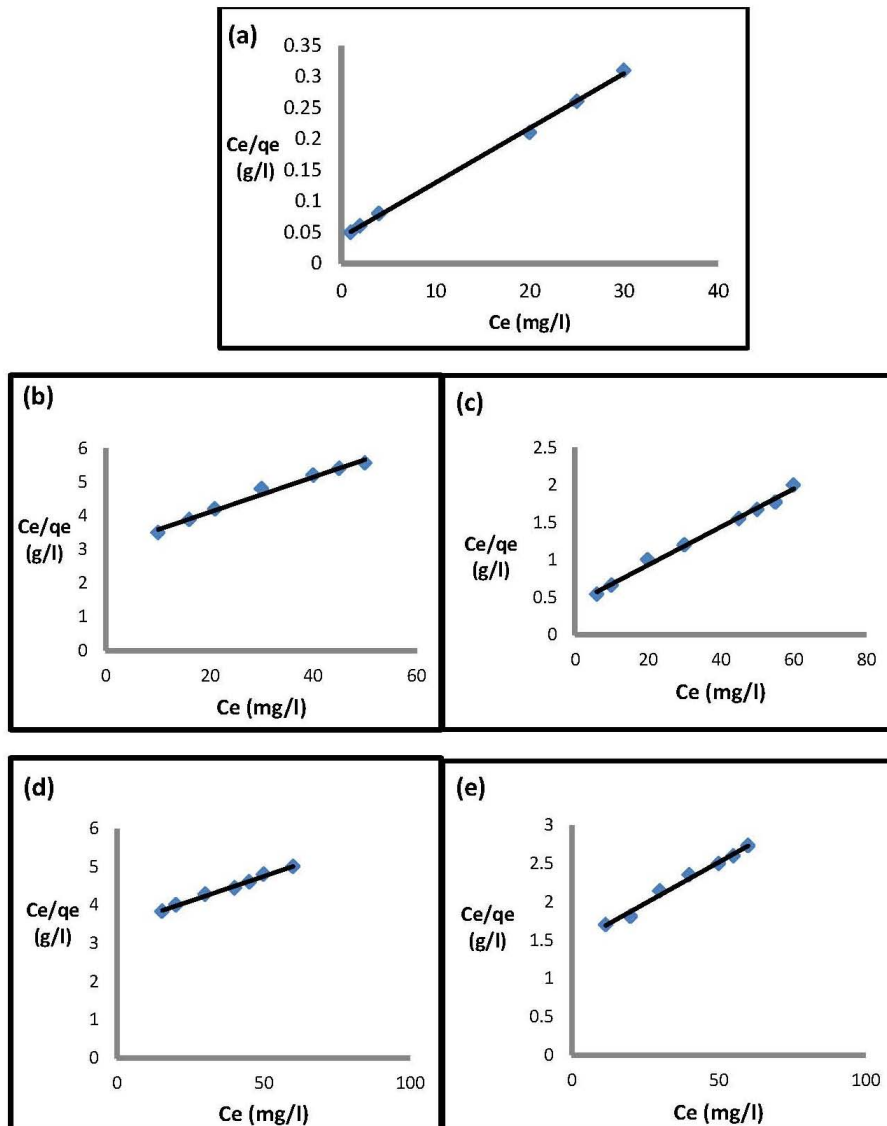


Fig. 8. Langmuir plots of MB adsorption onto : a) MWCNTs, b) o-Toluidine, c) MWCNTs/nanocomposite (o-Toluidine), d) m-Toluidine, e) MWCNTs/nanocomposite (m-Toluidine).

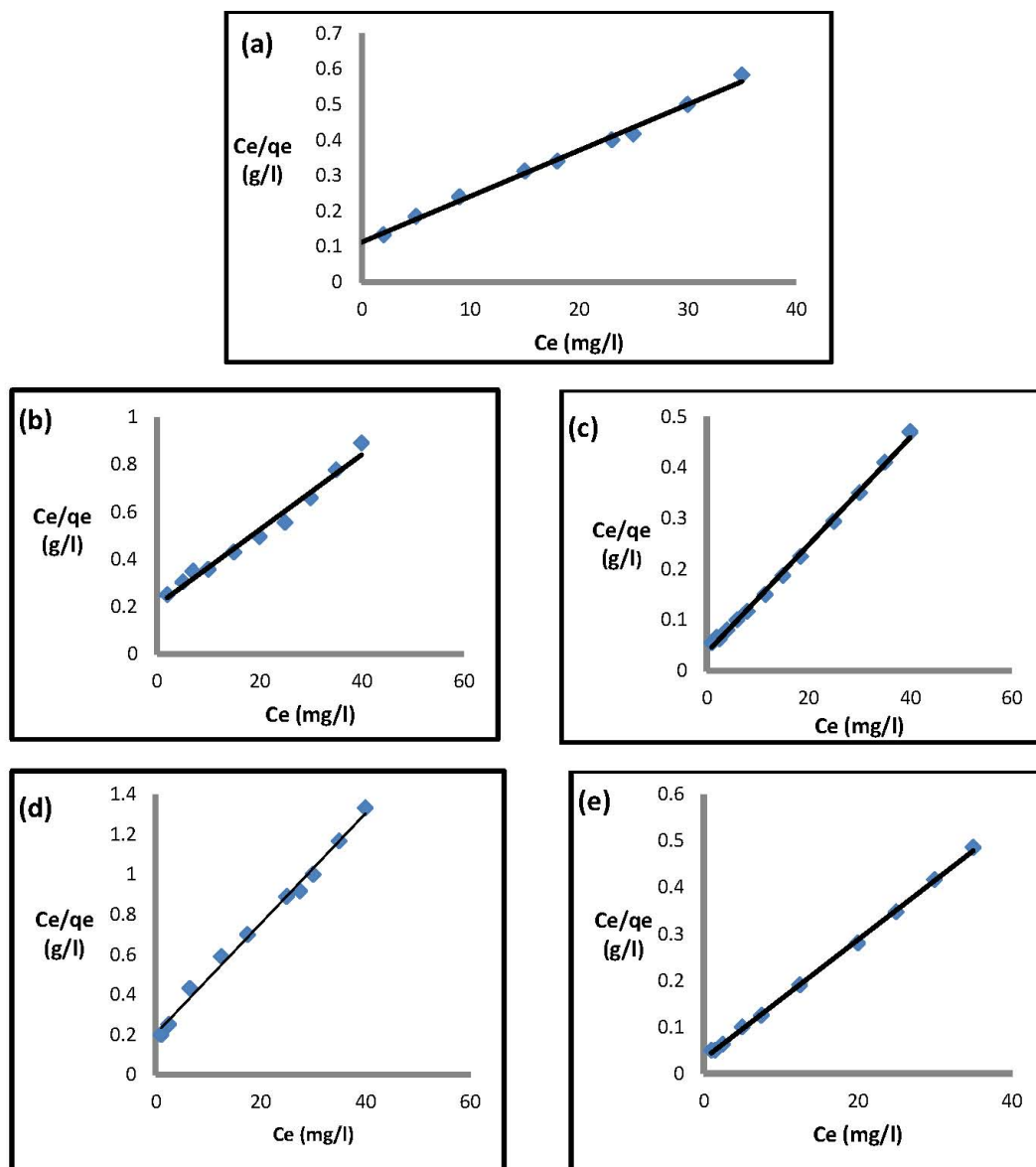


Fig. 9. Langmuir plots of Pb^{2+} adsorption onto: a) MWCNTs, b) o-Toluidine, c) MWCNTs/nanocomposite (o-Toluidine), d) m-Toluidine, e) MWCNTs/nanocomposite (m-Toluidine).

References

1. **Sundaramurthy, J., Li, N., Kumar, P.S. and Ramakrishna, S.**, Perspective of electrospun nanofibers in energy and environment, *Biofuel Research Journal*, **1**, 44-54 (2014).
2. **Liu, Q. , Nayfeh, M.H. and Yau, S.T.**, Brushed-on flexible supercapacitor sheets using a nanocomposite of polyaniline and carbon nanotubes. *Journal of power sources*, **195**, 7480-7483(2010).
3. **Thostenson, E.T. and Chou, T.W.**, Processing-structure-multifunctional property relationships in carbon nanotubes epoxy composites. *Carbon*, **44**, 3022-3024(2006).
4. **Lu, X., Zhang, W., Wang, C., Wen, T.C. and Wei, Y.**, One – dimensional conducting polymer nanocomposites: Synthesis, properties and applications, *Progress in Polymer Science*, **36**(5), 671-712 (2011).
5. **Zhang, W.D. and Zhang, W.H.**, Carbon nanotubes as active components for gas sensors. *Journal of Sensors*, Article. ID 160698, 16 pages (2009).
6. **Chen, Y., Gan, C., Zhang, T., Yu, G., Bai, P. and Kaplan, A.**, Laser-surface-alloyed carbon nanotubes reinforced hydroxyapatite composite coatings. *Applied Physics Letters*, **86** (1 – 3), Article ID 251905(2005).
7. **Pradhan, D. and Sharon, M.**, Carbon nanotubes, nanofilaments and nanobeads by thermal chemical vapor deposition process. *Material Science and Engineering*, **96**, 24-28 (2002).
8. **Kasiraman, G., Nagalingam, B. and Balakrishnan, M.**, Performance, emission and combustion improvements in a direct injection diesel engine using cashew nut shell oil as fuel with camphor oil blending, *Energy*, **47**, 116-124 (2012).
9. **Nagaraju, N., Fonseca, A., Konya, Z. and Nagy, J.B.**, Alumina and silica supported metal catalysts for the production of carbon nanotubes. *Journal of Molecular Catalysis A*, **181**, 57–62 (2002).
10. **Ago, H., Nakamura, K., Uehara, N. and Tsuji, M.**, Roles of metal-support interaction in growth of single-and double-walled carbon nanotubes studied with diameter-controlled iron particles supported on MgO. *Journal of Physical Chemistry B*, **108** (49), 18908- 18915 (2004).
11. **Jeon, I.Y., Tan, L.S. and Baek, J.B.**, Synthesis and electrical properties of polyaniline/ polyaniline grafted multiwalled Carbon nanotube mixture via in situ static interfacial polymerization, *Journal of polymer science, Part A: Polymer Chemistry*, **48** , 1962 – 1972 (2010).
12. **Pandi, G. and Ramaiah, S.**, Polyaniline-carbon nanotube composites. *Pure Appl. Chemistry*, **80**, 2377 (2008).
13. **Luo, Y.C. and Do, J.S.**, Urea biosensor based on PANI (urease) Nafion/Au composite electrode. *Biosensors and Bioelectronics*, **20**, 15-23 (2004).

14. **Odom, T.W., Huang, J.L., Kim, P. and Lieber, C.M.,** Atomic structure and electronic Properties of Single-walled Carbon Nanotubes. *Nature*, **391**, 62 (1998).
15. **Tehrani, M.S., Azar, P.A., Namin, P.E. and Deghaghi, S.M.,** Removal of lead ions from wastewater using functionalized multiwalled carbon nanotubes with tris(2-aminoethyl)amine. *J. of Env.Protection*, **4**, 529-536(2013).
16. **Narzihah, A.H., Fakhru-Razi, A., Thomas, S.Y., Choong and Chuah, L.,** Surface modification effects on CNTs adsorption of methylene blue and phenol. *J. of Nanomaterials*, doi: 10.1155/2011/495676. Article ID 495676, 18 pages (2011).
17. **Sabelo, D.M., Kartick, C.M., Robin, C., Michael, J.W. and Neil, J.C.,** The effects of Synthesis Parameters on the catalytic synthesis of multiwalled carbon nanotubes using Fe-Co/CaCO₃ catalysts. *South African Journal of Chemistry*, **62**, 67-76 (2009).
18. **Hao, Y., Qunfeng, Z., Fei, W., Weizhong, Q. and Guohua L.,** Agglomerated CNTs synthesis in a fluidized bed reactor: agglomerate structure and formation mechanism. *Carbon*, **41**, 2855-2863 (2003).
19. **Yang, J., Ray, I.,** Frost synthesis and characterization of boehmite nanofibers, *Research Letters in inorganic Chemistry*, ID 602198. DOI: 10.1155//602198 (2008).
20. **Angulakshmi, V.S., Karthikeyan, S. and Syed Shabudeen, P.S.,** Effect of synthesis temperature of the growth of MWCNTs from ZEAMAYS oil as evidenced by structural, Raman and XRD analysis. RAS ĀYAN. *Journal of Chemistry*, **8**, 1-7 (2015).
21. **Maser, W.K., Benito, A.M., Callejas, M.A., Seegar, T., Martinez, M.T., Schreiber, J., Muszynski, J., Chauvet, O., Osvath, Z., Koós, A.A. and Biró, L.P.,** Synthesis and characterization of new polyaniline /nanotube composites. *Materials Science and Engineering C.*, **23**, 87-91(2003).
22. **Ateih, M.A., Bakather, O.Y., AL-Tawbini ,B., Bukhari, A.A., Abuilawi, F.A. and Fettouhi, M.B.,** Effect of carboxylic functional group functionalized on carbon nanotubes surface on the removal of lead from water, *Bioinorganic Chemistry and applications*, article ID: 603978, 9PAGES (2010).
23. **Youssef, A.T., Bagheri, S., Shinji, K., Rouhi, J. and Mahmood ShoichriIkedo, M.R.,** Fast synthesis of MWCNTs from Camphor Oil as an energy Storage material. *Bio Med Research International*, Article.ID.691537, 6 PAGES(2014).
24. **Kandawar, S.B., Anwane, S.W., Nandanwar, D.V. and Dhakate, S.R.,** CNTs reinforced conducting polyaniline and its derivative poly (o-anisidine) composites. *Advances Material Letters*, **4**(1), 35-38 (2013).
25. **Jahangiri, M., Kiani, F., Tahermansouri, H. and Rajabalinezhad, A.,** The removal of lead ions from aqueous solutions by modified multi – walled carbon nanotubes with 1 – isatin – 3 – thiosemicarbazone. *Journal of Molecular Liquids*, **212**, 219 - 226 (2015).

26. **Zhu, J., Jia, J., Kwong, F.L., Leung, Ng, D.H. and Tjong, S.C.**, Synthesis of multiwalled carbon nanotubes from bamboo charcoal and the role of minerals on their growth, *Biomass and Bioenergy*, **36**, 12 – 19(2012).
 27. **Qiu, B., Xu, C., Sun, D., Wei, H., Zhang, X., Guo, J., Wang, Q., Rutman, D., Wei, S. and Guo, Z.**, Polyaniline coating on carbon fiber fabrics for hexavalent chromium removal, *RSCAdv*, **4**, 29855 – 29865 (2014).
 28. **Stejskal, J., Kratochvil, P. and Radhakrishnan, N.**, Polyaniline dispersions 2. UV-Vis absorption spectra, *Synthesis Metals*, **61**, 225-231 (1993).
 29. **Scherr, E.M., Mac Diarmid, A.G., Manahar, S.K., Masters, J.G., Sun, Y. and Tang, X.**, Polyaniline – oriented films and fibers. *Synth.Met.*, **41**(1),735 (1991).
 30. **Xia, H. and Wang, Q.**, Preparation of conductive polyaniline/nanosilica particle composites through ultrasonic irradiation, *Journal of Applied Polymer Science*, **87**(11), 1811(2003).
 31. **Langmuir, I.**, The constitution and fundamental properties of solids and liquids. *J. Am. Chem. Soc.*, **38**, 2221 – 2295 (1916).
 32. **Freundlich, H.M.F.**, Over the adsorption in solution. *J.Chem.*, **57**, 385 – 471 (1906).
 33. **Yao, Y., Xu, F., Chen, M., Xu, Z. and Zhu, Z.**, Adsorption behavior of methylene blue on carbon nanotubes, *Bioresource Technology*, **101**, 3040 – 3046 (2010).
 34. **Weng, C.H.**, Modeling Pb(II). Adsorption onto Sandy Loam Soil. *J. of Colloid and Interface Science*, **272**, 262-270 (2004).
 35. **Ekrumul Mahmud, H.N.M., Hosseini, S. and Yahya, R.B.**, Polymer adsorbent for the removal of lead ions from aqueous solution. *International J. of Technical Researsch and Applications*. **11**, 4-8 (2014).
 36. **Chang, P.R., Zheng, P., Liu, B., Anderson, D.P., Yu, J. and Ma, X.**, Characterization of magnetic soluble starch-functionalized carbon nanotubes and its application for the adsorption of the dyes. *J. Hazard. Mater.*, **186**, 2144–2150 (2011).
 37. **Gonga, J.L., Wanga, B., Zenga, G., Yanga, C.P., Niua, C.G., Niua, Q.Y., Zhoua, W.J. and Liang, Y.**, Removal of cationic dyes from aqueous solution using magnetic multi-wall carbon nanotube nanocomposite as adsorbent. *J. Hazard. Mater.*, **164**, 1517–1522 (2009).
 38. **Madrakiana, T., Afkhamia, A., Ahmadia, M. and Bagheri, H.**, Removal of some cationic dyes from aqueous solutions using magnetic-modified multi-walled carbon nanotubes. *J. Hazard. Mater.*, **196**, 109–114 (2011).
 39. **Tehrani, M.S., Azar, P.A., Naming, P.E. and Dehaghi, S.M.**, Removal of lead ions from aqueous solution using multi-walled carbon nanotubes: The Effect of functionalization. *J. Appl. Environ. Biol. Sci.*, **4**(2), 316-326 (2014).
 40. **Mamba, G., Mbianda, X.Y., Govender, P.P., Mamba, B.B. and Krause, R.W.**, Application of multiwalled carbon nanotube-cyclodextrin polymers in the removal of heavy metals from water. *J.Appl.Sci*, **10**(11), 940-945(2010).
- Egypt. J. Chem.* **60**, No.2 (2017)

(Received 16/1/2017;
Accepted 9/3/2017)

اقتناص صبغة الميثيلين الأزرق وإيونات الرصاص من المحاليل المائية بواسطة انابيب الكربون النانومترية المطعمة ببعض البوليمرات الموصلة للكهرباء

أمينة عبد المجيد عطية¹، منى عبد الحميد شومان¹، السعيد محمود احمد الصباح²، نادي عطية فتحي¹، امجد بهيج خليل²، خديجة محمد عباس¹
¹قسم الكيمياء الفيزيائية- معمل كيمياء السطوح و الحفز- المركز القومى للبحوث و² قسم الكيمياء-كلية العلوم-جامعة بنى سويف - مصر.

مع الاخذ بعين الاعتبار المبادئ القائمة للكيمياء الخضراء جرت محاوله لانتاج كربون نانومتري ذو كفاءه عاليه من مواد متجدده وصادقه للبيئه .انابيب الكربون النانومترية لها خصائص عاليه مثل مساحه السطح وسهله التوظيف وتتميز بخصائص ميكانيكيه ، حراريه وكهربائيه فريده من نوعها جعلها عنصرا جذابا للمترابطات مما ادي الي جذب اهتمام كبير الي انتاج المترابطات النانومترية . فقد تم تركيز العمل البحثي علي تحضير انابيب الكربون النانومترية من نبات الكافور من خلال محفز نترات الحديد يدعمه اسلوب التثريب الرطب علي الالومينا كدعامه . وصفت عينات الكربون النانومترية وايضا مركبات انابيب الكربون النانومترية المطعمة ببوليمرات (o , m toluidine) المحضره من خلال الميكروسكوب الالكتروني النافذ (HRTEM) ' حيود الاشعه السينيه (XRD) ' التحليل بواسطة امتصاص الاشعة دون الحمراء (FTIR) ' تحليل امتصاص الاشعة فوق البنفسجية (UV-Vis)' التركيب المسامي للعينات المحضرة و التحليل الحرارى (TGA).

و قد أظهرت النتائج أن عينات انابيب الكربون النانومترية امتصت كميات كبيرة من صبغة الميثيلين الأزرق عن المترابطات النانومترية بينما اظهرت المترابطات النانومترية كفاءة عالية في امتصاص ايونات الرصاص Pb^{+2} .

مما سبق يتضح أن انابيب الكربون النانومترية و تكوين مترابطات نانومترية لها امكانيات كبيرة كمواد واعدة للتطبيق في الامتزاز من المحاليل المائية.